Computers in Biology and Medicine 159 (2023) 106697

Contents lists available at ScienceDirect

Computers in Biology and Medicine

journal homepage: www.elsevier.com/locate/compbiomed

Development of a novel low-order model for atrial function and a study of atrial mechano-electric feedback

Nicholas F. Pearce [a,*], Mark C. Turner [b], Helen L. Maddock [b], Eun-jin Kim [a]

[a] Fluids and Complex Systems Center, Faculty of Engineering, Environment and Computing, Coventry University, Coventry, CV1 5FB, UK
[b] Centre for Sport, Exercise and Life Sciences, Research Institute for Health and Well-being, Coventry University, Coventry, CV1 5FB, UK

ARTICLE INFO

Keywords:
Nonlinear dynamics
Multi-scale model
Atrium
Cardiac cycle
Mechano-electric feedback
Lumped-parameter model

ABSTRACT

Numerical models of the cardiovascular system have largely focused on the function of the ventricles, with atrial function often neglected. Furthermore, the time-varying elastance method that prescribes the pressure–volume relationship rather than calculating it consistently is frequently used for the ventricles and atrium. This method has yet to be validated however, so its applicability for cardiac modelling is frequently questioned. To overcome this challenge, we propose a synergistic model of left atrium (LA) and left ventricle (LV) by self-consistently integrating various feedback mechanisms among the electro-mechanical and chemical functions of the micro-scale myofiber, the macro-scale dynamics of the LA and LV, the atrioventricular node (AV), and circulation. The model is tested and shown to reproduce the essential features of the atrium cycling, such as the characteristic figure of eight pressure–volume loops. Our model is further developed to investigate the effect of dysfunctions of the mechanical-electric feedback (MEF) in the atrium. Our model not only successfully reproduces key experimental MEF observations such as prolonged action-potential and increases in action-potential magnitude induced by atrial stretch but also shows how MEF and arrhythmia of the atrium lead to a degradation of cardiac output and pumping power with significant consequences. In particular, MEF reproduces arrhythmia such as ectopic and erratic cycling, missed heart beats and restricted function.

1. Introduction

Cardiac disease remains one of the leading causes of death worldwide [1] and atrial fibrillation (AFib), an irregular rhythm in the atrium, is responsible for many of these deaths. In the US alone, AFib was responsible for around 26,535 deaths [2] and untreated AFib or atrial flutter frequently leads to strokes and heart failure [3]. The left atrium (LA) plays a crucial role in the cardiovascular system and goes through three distinct phases during the cardiac cycle; a passive blood reservoir phase during ventricular systole, followed by the conduit phase when the mitral valve opens allowing the collected blood to flow into the ventricle, ending with an active contraction phase after which the mitral valve closes. This multi-phasic behaviour of the atrium leads to the double-loop pattern displayed by the atrial pressure–volume diagram, with the loops representing the active 'a-phase' and passive 'v-phase' of the atrial cycle.

Numerical models of the cardiovascular system have often overlooked the behaviour and importance of the LA [4], or invoked the time-varying elastance (TVE) method to simulate it [5–7]. The TVE method uses physiological data to tune a periodic function of time describing the pressure–volume relation of the left ventricle (LV) or atrium. Despite the popularity of the TVE approach, its accuracy is frequently questioned and criticised due to its empirical foundations [8,9]. A main drawback of the TVE approach is the neglect of physiological feedback mechanisms which consistently regulate pressure, volume and circulation. Consequently, it is unsuitable for modelling various pathologies and clinical interventions such as left ventricle assist devices (LVADs) and cardiac fibrillation. Various attempts have been made to improve or overcome the deficiencies of the TVE method where such feedback is important: the atrioventricular interaction and valve motion have been included [4,10]; the electrical dynamics of the heart chambers have been modelled to complement the mechanical chambers [10]; Gaussian functions have been used to drive the TVE [10]; and time-varying muscle mechanics with a constant elastance used in place of a TVE [11], which assumes that atrial pressure changes according to its volume. A further weakness of the TVE approach is its dependence on the loading conditions when used for the atrium [12,13] motivating to the development of an alternative method entirely by Pironet et al. [9]. Their multi-scale method is reliant on empirical data though, and uses the TVE method to model the remaining cardiovascular system. CFD software has also be applied [14], however

* Corresponding author.
E-mail address: pearcen5@uni.coventry.ac.uk (N.F. Pearce).

https://doi.org/10.1016/j.compbiomed.2023.106697
Received 28 September 2022; Received in revised form 1 February 2023; Accepted 14 February 2023
Available online 17 February 2023
0010-4825/© 2023 The Author(s). Published by Elsevier Ltd. This is an open access article under the CC BY license (http://creativecommons.org/licenses/by/4.0/).

CFD software is very costly in terms of time and computational power, making it inaccessible in a clinical environment.

The mechano-electric feedback mechanism (MEF) is one of the many feedback systems at work in the heart to maintain stability and proper cardiac function. It is the sensitivity to mechanical stimulation at the cellular level which induces an electrical response. The excitation-contraction coupling (ECC) operates in the other 'direction', i.e. a mechanical response at the cell level induced by electrical stimulation. Whilst the MEF mechanism helps to coordinate mechanical and electric activities among the countless cardiac cells [15], it can have some important and often dangerous consequences. The effects of the MEF on the ventricle have been well-documented and investigated using experimental and numerical approaches (see for example, the extensive reviews by Quinn and Kohl [15] and Quarteroni [16]). Among the many actors thought to be responsible for the MEF, stretch induced ion channels (SACs) are the main contenders [17,18]. These channels respond to mechanical stretch by opening and closing, allowing the conduction or block of ions into the cell. Stimulating these channels can thereby change the character of the action potential: the electrical wave that causes cell contraction and relaxation. The action potential changes depend on the period in the cardiac cycle at which stretch is induced. For the ventricles, cell stretch during ventricular systole can reduce the action potential duration [19–21]. Stretch during diastole can depolarise the cell, causing ectopic excitation [22].

The consequences of the MEF for the atrium have been investigated experimentally by Solti et al. [23] who use atrial balloon inflation to dilate the left atria of anaesthetised dogs. Atrial arrhythmia can be induced more readily and spontaneous tachycardia occurs when the atrium is stretched. By attaching electrodes to the atrium, electrophysiological effects can be manipulated. Stretch causes the refractory period in the atrium tissue to fall and the conduction time to increase. Decreased conduction velocity and shortening of the refractory period are also seen by Chorro et al. [24] in perfused rabbit hearts, and atrial fibrillation by dilation has been confirmed experimentally by [25–27]. Fibrillation susceptibility rise has been observed in humans with dilated atria [28], and the modulation of conduction velocity has been confirmed in people too [29]. Although computer modelling has been used extensively to explore ventricular MEF function, only a limited amount of work is devoted to the MEF modelling for the atrium such as the cellular-scale study by Brocklehurst et al. [30].

The main aim of this paper is to develop a consistent model of the LA and LV and study MEF based on the synergistic model of the LV in Kim and Capoccia [31,32]. In the adopted approach, a model of the myofiber contraction is used to control ventricular dynamics. This is combined with a model of circulation on the macro-scale to form a multi-scaled representation of cardiac function. Pressure and volume are thereby calculated consistently, allowing feedback mechanisms to operate, negating the need to apply the TVE approach. This synergistic method is similar to that used by Pironet et al. [9] in that the micro-scale and macro-scale are coupled, but does not rely on empirical data to function. Using our new model allows one of the first (to the authors knowledge) explorations of MEF in the LA to be made. Our model is developed to allow clinicians to easily investigate the effects of drugs and other interventions on the pressure, volume and circulation and vice-versa. A further advantage of our model is that measurements of patient data can be used to create patient specific models. Identification of appropriate treatment can also be made by integrating our model with deep-learning techniques or similar such adaptive methods [33,34]. The synergistic model of LV was validated as a TVE alternative in [31] and has previously been used to study Left Ventricle Assist Device (LVAD) function [31] as well as various pathologies such as dilated cardiomyopathy. Ventricular MEF was investigated in [32,35] reproducing MEF effects consistent with the findings by other authors, such as longer action potential duration consistent with [36]. Electrical patterns revealed ectopic peaks along with rapid oscillation in agreement with [17,37,38] showing the effect of SACs. The rest of the paper is organised as follows: in Section 2 the numerical model is described; in Section 3, the results for the control case and MEF examination are presented; the results are discussed in Section 4; and in Section 5, a conclusion to this study is provided.

2. Materials & methods

Here, the development of our synergistic model of the LA and LV is described. Our LA model combines the micro-scale myocyte dynamics and macro-scale circulation dynamics, pressure, and volume relations using a similar approach to the LV model in Kim and Capoccia [31,32]. The evolution of the LA and LV is coupled at the macro-scale through circulation dynamics since the atrium model feeds blood to the left ventricle through the mitral valve and receives the returning blood from the systemic circulation. As detailed by Walklate et al. [39] some key differences in the atrium are as follows: the myocyte density in the ventricles is greater than the atria and the myocytes are larger in volume, wider and have a different shape (rod shaped), resulting in a 30 to 50% greater tension developed by the ventricle myocytes than those in the atrium. Another difference is in the contraction amplitude. In both LV and LA, contraction amplitude is influenced by the level of calcium activation. The atrial calcium cycling is faster than the ventricular one due to excitation-contraction coupling protein differences and their different sarcoplasmic reticulum structural features. The calcium in the atrium consequently decays faster than the ventricle resulting in a greater duration of the ventricle contraction cycle. Some of these differences are reflected in the model presented below using different model parameters (Tables 1 and 2).

2.1. The ventricle micro-scale electro-mechanical model

The Bestel-Clement-Sorine [40,41] approach is employed to simulate the LV myofiber function. This approach is based on the Hill-Maxwell rheological representation of the myofiber. In this design the electrically activated sarcomere element is modelled by coupling an active contractile element in series with another elastic element allowing active relaxation. These sarcomere elements function in parallel to a third elastic element representing the passive connective tissues surrounding the sarcomere, and stopping the heart exceeding its limits [42]. The active contractile element mechanics of the ventricle are modelled by the governing equations below for active (represented using the subscript 'c') stress τ_c, strain ϵ_c, stiffness k_c, and velocity $v_c = \frac{d\epsilon_c}{dt}$.

$$\frac{dv_c}{dt} = -\chi v_c - \omega_0^2 \epsilon_c - a\tau_c d_0(\epsilon_c) + b\left(\sqrt{\frac{V}{V_0}} - 1\right) \tag{1}$$

$$\frac{d\epsilon_c}{dt} = v_c \tag{2}$$

$$\frac{d\tau_c}{dt} = k_c v_c - (a_l|v_c| + |u|)\tau_c + \sigma_0 u_+ \tag{3}$$

$$\frac{dk_c}{dt} = -(a_l|v_c| + |u|)k_c + k_0 u_+ \tag{4}$$

$$d_0(\epsilon_c) = e^{-\beta_0(\epsilon_c - 0.1)^2} \tag{5}$$

The subscript '+' means that only positive values of the preceding term are used. On the right hand side of Eq. (1) the first term $\chi\tau_c$ is a damping force. The second term $\omega_0^2\epsilon_c$ is the harmonic force with frequency ω_0^2. The third term $a\tau_c d_0(\epsilon_c)$ is an active force and the final term $b(\sqrt{V/V_0} - 1)$ is a passive force. u represents the time-varying calcium bound Troponin-C concentration responsible for cell activation. The final equation for $d_0(\epsilon_c)$ represents the Frank-Starling effect of cell stretching. It is modified here to be more representative of cell stretch, peaking now at a positive value [42,43]. χ, a, b, α_l and β_0 are positive constants. σ_0 and k_0 are constants too and represent the maximum cell stress and stiffness. The stress directed by the passive elastic element is assumed to be exponential [44] and is given by the equation below.

$$\sigma_p = \frac{k_2}{k_1}[\exp(k_1(\sqrt{V/V_0} - 1)) - 1] \tag{6}$$

Here, k_1, k_2, and V_0 are positive constants. The passive element in Eq. (1) and σ_p in Eq. (6) are derived from a radially contracting cylinder with constant height. The strain ϵ is therefore proportional to the square root of the ventricle cylinder volume $\sqrt{V}$.

2.2. The atrium micro-scale model

To simulate the atrial myocyte contractile mechanics, an identical set of equations to the ventricle above are used with different parameters. The variables and parameters of the atrium are identified using a subscript 'A'. The equations therefore read,

$$\frac{dv_A}{dt} = -\chi_A v_A - \omega_{0A}^2 \epsilon_A - a_A \tau_A d_{0A}(\epsilon_A) + b_A \left(\sqrt{\frac{V_A}{V_{0A}}} - 1 \right) \tag{7}$$

$$\frac{d\epsilon_A}{dt} = v_A \tag{8}$$

$$\frac{d\tau_A}{dt} = k_A v_A - (a_{lA}|v_A| + |u_A|)\tau_A + \sigma_{0A} u_{A+} \tag{9}$$

$$\frac{dk_A}{dt} = -(a_{lA}|v_A| + |u_A|)k_A + k_{0A} u_{A+} \tag{10}$$

$$d_{0A}(\epsilon_{cA}) = e^{-\beta_{0A}(\epsilon_A - 0.1)^2} \tag{11}$$

$$\sigma_{pA} = \frac{k_{2A}}{k_{1A}} [\exp(k_{1A}(\sqrt{V_A/V_{0A}} - 1)) - 1] \tag{12}$$

β_{0A} is identical in value to β_0 such that the same Frank-Starling relation applies in both ventricle and atrial muscle cells.

2.3. The macro-scale pressure

The micro-scale myofiber mechanics cause the expansion and contraction of the atrium and ventricle. The governing equation of the macro-scale ventricular pressure reads,

$$P_V = \gamma \frac{V_0}{V} [d_0(\epsilon_c)\tau_c + \sigma_p] \tag{13}$$

Likewise for the atrium,

$$P_A = \gamma_A \frac{V_{0A}}{V_A} [d_{0A}(\epsilon_{cA})\tau_{cA} + \sigma_{pA}] \tag{14}$$

where γ is the ratio of ventricular wall thickness to the radius and γ_A the same for the atrium. These equations embody the connection between the micro and macro scales.

2.4. The circulation model

We extend the full circulation model of Kim and Capoccia by using the atrial pressure determined by Eq. (14). The governing equations for chamber volumes V, V_A, aortic pressure m and flow F_a, and the arterial pressure P_s read,

$$\frac{dV}{dt} = \frac{1}{R_m}(P_A - P_V)_+ - \frac{1}{R_a}(P_V - m)_+ \tag{15}$$

$$\frac{dm}{dt} = -\frac{F_a}{C_a} + \frac{(P_V - m)_+}{C_a R_a} \tag{16}$$

$$\frac{dF_a}{dt} = \frac{m - P_s}{L_s} - \frac{R_c F_a}{L_s} \tag{17}$$

$$\frac{dP_s}{dt} = \frac{1}{C_s R_s}(P_A - P_s) + \frac{F_a}{C_s} \tag{18}$$

$$\frac{dV_A}{dt} = \frac{1}{R_s}(P_s - P_A) - \frac{1}{R_m}(P_A - P_V)_+ \tag{19}$$

Here, C_a and C_s are the aortic and systemic compliance, L_s is the aortic blood inertance and R_m, R_a, R_s, and R_c are the mitral valve, aortic, systemic and characteristic resistances, all of which are positive constant.

2.5. The electro-chemical model

The cellular electrical and chemical activity drive contraction and relaxation of the sarcomere. Huxley [45] was one of the first to develop a model for the propagation of cell neural electrical excitation (action potential). Since then, many models of varying complexity have been proposed to express cell activity (see [18,19,46] for example). Here, the simplified FitzHugh–Nagumo neural model is used [47]. This model has two (dimensionless) variables; one describing the slow electrical response p, and one describing the fast q. Although they do not correspond to individual ion currents, the passage of ion currents would affect the MEF parameter values, as used in the previous works [31,32,35]. Thus in this respect, they qualitatively capture ion channel effects. The governing equations for the ventricle read

$$\frac{dp}{dt} = 0.1(q - p + \mu_1 \tau_c) \tag{20}$$

$$\frac{dq}{dt} = 10q(1 - q^2) - 10(2\pi)^2 p + \mu_2 V_+ + 10 q_A(t + s) \tag{21}$$

$$u = \alpha_u q \tag{22}$$

As described above, Eq. (22) for u represents the chemical activity. The governing equations for the atrium take a similar form.

$$\frac{dp_A}{dt} = 0.1(q_A - p_A + \mu_{1A}\tau_A) \tag{23}$$

$$\frac{dq_A}{dt} = 10q_A(1 - q_A^2) - 10(2\pi)^2 p_A + \mu_{2A} V_{A+} + 10\cos(2\pi t) \tag{24}$$

$$u_A = \alpha_{uA} q_A \tag{25}$$

The slow variables p and p_A mimic the slower repolarisation phase of the excitation wave. The faster variables q and q_A mimic the faster depolarisation phase so are linked to the chemical excitation equation for u ($u > 0$ during contraction, $u < 0$ during relaxation). Note that in [32] the slow variables p and p_A are linked to the action potential. The parameter α_u and similarly α_{uA} are positive constants. The last term in Eq. (24) is an oscillating force that simulates signals from the sino-atrial (SA) node. These signals reach the atria first, then pass to the AV node before propagating to the ventricles. The AV node plays a number of roles and provides the only conduction pathway between the atria and ventricles [48], hence the SA term in Eq. (24) is replaced with $10q_A(t + s)$ in Eq. (21). The parameter s is a timing parameter used to set the difference between atrial and ventricle contraction. μ_1 and μ_2 are the MEF parameters for the LV and μ_{1A} and μ_{2A} are for the LA. As their names describe, they are the influence of the mechanical activity on the electrical. For comprehensive descriptions of these parameters see [32,35]. Briefly though, μ_1 (and μ_{1A}) describes the feedback of systolic mechanical stress (stretch) on the excitation wave by coupling p to τ_c (and p_A to τ_{cA}). μ_2 (and μ_{2A}) describes the feedback of diastolic stretch on the excitation wave by coupling $V > V_0$ to q ($V_A > V_{0A}$ to q_A). In the control case, $\mu_1 = 0.0024$ kpa^{-1}, and $\mu_2 = 0$ (s ml)$^{-1}$ and the same are used for the atrium.

The equivalent electrical diagram for the complete model just described is shown in Fig. 1 below. The physiological meaning of the model variables are given in Table 4. To help readers understanding our model, we show in Fig. 2 the multiscale nature of our synergistic model through coupling different activities.

2.6. Control case parameters

To demonstrate that the model properly accounts for the cardiovascular system, we fine-tune parameter values to obtain the results of a control case representing a healthy heart at rest, free of underlying pathologies. The parameter values for this control case are given in the Tables 1–3 below. Specifically, the values used for the ventricle micro-scale model are given in Table 1, and those for the atrium in Table 2. Values for the circulation can be found in Table 3. The system of Eqs. (1)–(25) are solved using a fourth-order Runge–Kutta

Table 1
Ventricle control parameters.

Parameter	Value	Physiological description
σ_0	240 kpa	Maximum left ventricle sarcomere active tension
k_0	120 kpa	Maximum left ventricle sarcomere active elastance
k_1,	0.002 kpa	Passive tension parameter
k_2	14 kpa	Passive tension parameter
χ, α_l	100 s^{-1}, 10 m^{-1}	Damping parameters
ω_0	100 s^{-1}	Micro-scale oscillation frequency
a, b	100 m s^{-2} kpa^{-1}, 6000 m s^{-2}	Active and passive tension parameters
β_0	$\frac{40}{3.5}$ ml^{-2}	Frank-starling length-tension parameter
γ	0.6	Left ventricle pressure parameter
V_0	$\frac{144}{1.5}$ ml	Left ventricle volume parameter
α_u	5 s^{-1}	Ventricle sarcomere chemical excitation parameter
μ_1, μ_2	0.0024 kpa^{-1}, 0 $(s\ ml)^{-1}$	Ventricle MEF parameters

Table 2
Atrium control parameters.

Parameter	Value	Physiological description
σ_{0A}	240 kpa	Maximum sarcomere active tension
k_{0A}	120 kpa	Maximum sarcomere active elastance
k_{1A},	0.002 kpa	Passive tension parameter
k_{2A}	9 kpa	Passive tension parameter
χ_A, α_{lA}	100 s^{-1}, 10 m^{-1}	Damping parameters
ω_{0A}	100 s^{-1}	Micro-scale oscillation frequency
a_A, b_A	1000 m s^{-2} kpa^{-1}, 1500 m s^{-2}	Active and passive tension parameters
β_{0A}	$\frac{40}{3.5}$ ml^{-2}	Frank-starling length-tension parameter
γ_A	0.6	Left atrium pressure parameter
V_{0A}	$\frac{144}{10}$ ml	Left atrium volume parameter
α_{uA}	2 s^{-1}	Atrium sarcomere chemical excitation parameter
μ_{1A}, μ_{2A}	0.0024 kpa^{-1}, 0 $(s\ ml)^{-1}$	Atrium MEF parameters
s	0.04 s	Atrium contraction timing parameter

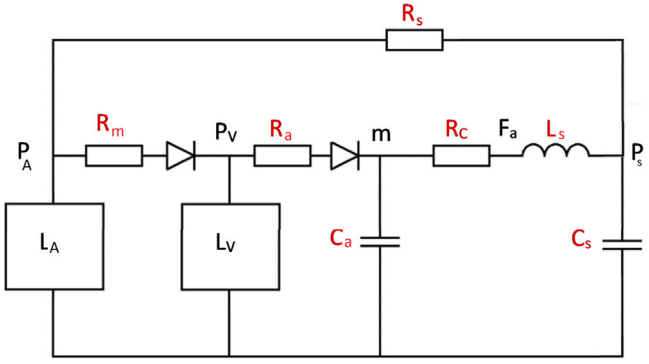

Fig. 1. The equivalent electrical diagram of the complete cardiovascular system described. For abbreviation definitions refer to Table 4. The left atrium LA feeds blood at a pressure P_A through the mitral valve (the first diode) into the left ventricle (LV). As the blood passes through the valve it encounters a resistance R_m. With the mitral valve closed the aortic valve (second diode) opens allowing blood at pressure P_V to flow into the aorta encountering a valve resistance R_a. The aorta has a compliance C_a. The aortic blood at pressure m flows (F_a) towards the remainder of the body encountering a characteristic resistance R_c. The blood has an inertia L_s due to its mass and encounters the resistance R_s and compliance C_s of the body's systemic arteries and tissues. The blood at pressure P_s after feeding the organs with fresh oxygen and nutrients is re-oxygenated and flows back to left atrium ready for another cycle.

scheme and the accuracy of the numerical solution is checked by systematically reducing the time-step until differences between results become negligible. All results were obtained using Matlab software. Whilst most of the initial model values have no to little effect on the result, the volumes of the ventricle and atrium do. For the control case, $V(0) = 135$ and $V_A(0) = 55$. The initial values of the ventricle variables are obtained by taking values from a ventricle-only model.

Table 3
Circulation parameters.

Parameter	Value	Physiological description
R_a	0.001 mmHg s/ml	Aortic valve resistance
R_m	0.005 mmHg s/ml	Mitral valve resistance
R_c	0.0398 mmHg s/ml	Characteristic resistance
R_s	0.5 mmHg s/ml	Systemic resistance
C_s	1.33 ml/mmHg	Systemic compliance
C_a	0.08 ml/mmHg	Aortic compliance
L_s	0.0005 mmHg s^2/ml	Inertance of blood in aorta

Table 4
Variables and their physiological meaning.

Variable	Physiological description
v_c	Velocity of the contractile element (s^{-1})
ϵ_c	Strain of the contractile element
τ_c	Active tension of the contractile element (mmHg)
k_c	Stiffness of the contractile element (mmHg)
σ_p	Passive stress (mmHg)
u	Chemical activity (s^{-1})
p	Slow electric variable
q	Fast electric variable
v_{cA}	Atrial micro-scale velocity (s^{-1})
ϵ_{cA}	Atrial strain of the contractile element
τ_{cA}	Active tension of the contractile element (mmHg)
k_{cA}	Atrial stiffness of the contractile element (mmHg)
σ_{pA}	Atrial passive stress (mmHg)
u_A	Atrial chemical activity (s^{-1})
p_A	Atrial slow electric variable
q_A	Atrial fast electric variable
P_V	Left ventricular pressure (mmHg)
P_A	Atrium pressure (mmHg)
P_S	Systemic pressure (mmHg)
m	Aortic pressure (mmHg)
V	Left ventricular volume (ml)
V_A	Left atrial volume (ml)

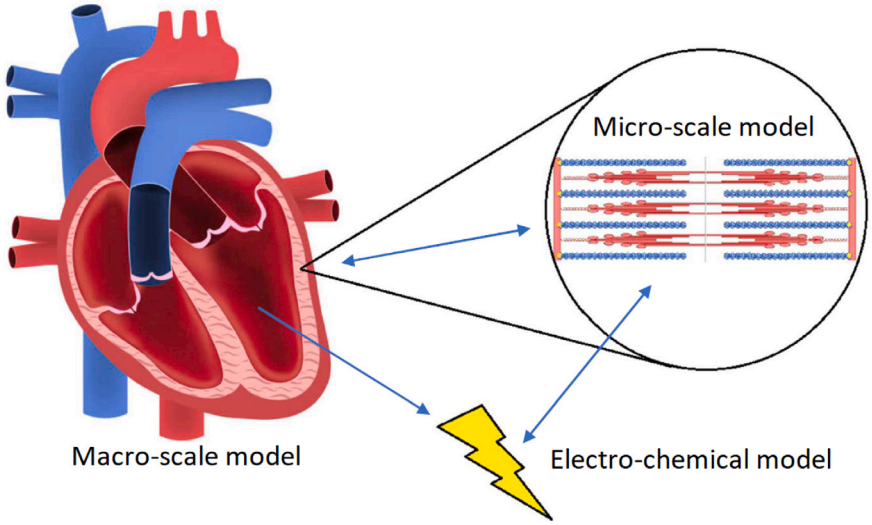

Fig. 2. An illustration of the our synergistic model.

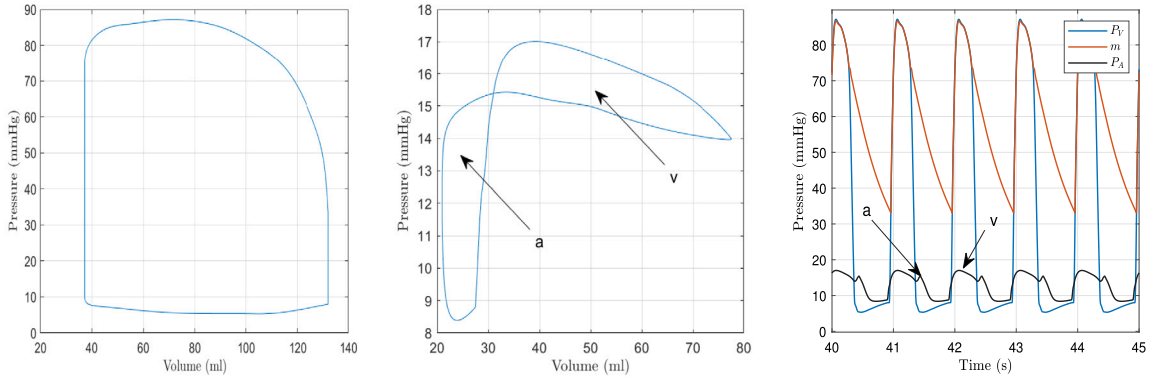

(a) Ventricle pressure-volume (b) Atrial pressure-volume loop (c) Time traces of the ventricular, atrial, and aortic pressures.

Fig. 3. Pressure–volume loops of the ventricle (3(a)) and atrium (3(b)). 3(c) shows time traces of the ventricle (blue), atrium (black) and aorta (red) pressures. The labels denote the passive 'v' phase and active 'a' phases.

3. Results

3.1. Control case results

3.1.1. Pressure–volume relation

We solve Eqs. (1) to (25) using the parameters given in Tables 1–3 for the control case and present the results after removing initial transients. The ventricle pressure–volume loop for the control case parameters given in the tables above is shown in Fig. 3(a). The stroke volume is 95 ml, and the power output is 0.93 W. The atrium pressure–volume loop is shown in Fig. 3(b). Whilst the pressure is typical of the atrium, the volume is greater than normally observed for a typical healthy human atrium, which is around 40 ml. The model has a large number of parameters requiring definition in order to function correctly. It is observed too that changes in the atrium parameters has a direct effect on the ventricle and vice-versa. A different set of parameter values may result in a lower atrial volume. However, with the chosen parameter values our model successfully reproduces the double-loop character of the atrium pressure–volume loop with the correct direction of the trace; a clockwise passive v-loop and an anticlockwise active a-loop. The simulated atrium, ventricle and aortic pressures for two cardiac cycles are shown in Figs. 3(c). It can be seen that the minimum between the v and a phases is not large due to the appearance of the a-phase early during ventricle diastole. This is why the a-loop in the atrium pressure–volume figure appears distended downward.

The time-evolution of other ventricle and atrium variables are shown in Fig. 4. The ventricle variables are displayed on the left and the atrium variables on the right. The strains ϵ_c and ϵ_{cA} and the change in volume V/V_0 and V_A/V_{A0} are shown in Figs. 4(a) and 4(d). Figs. 4(b) and 4(e) show the stresses τ_c and τ_{cA} with the stiffness k_c and k_{cA}. In Figs. 4(c) and 4(f), the slow and fast variables from the electrical model are displayed. Among all these figures, the main difference is found to be between ϵ_c and ϵ_{cA}. In particular, ϵ_{cA} has a 2-phase character reflecting the 2-phase nature of the atrium.

3.1.2. Preload reduction and the ESPVR

The individual atrial and ventricular preloads are now gradually reduced to obtain the end-systolic pressure–volume relationships (ESPVR) (Fig. 5). The plotted line crosses the minimal systolic volume of each loop. The line can be seen to cross the volume axis (at 0 pressure) at around 5 ml. The same result for the atrium is shown in Fig. 5(b), obtained through increases in atrial preload.

The minimum atrium volume that identifies the atrium end systole [49] is found and shown by the crosses on each loop in Fig. 5(b). An approximately linear reduction is found like the ventricle for the lower four points atrium until the preload reaches 90%. The least squares method was used to plot the ESPVR for the atrium using the lower 4 data marks, and is shown by the line in Fig. 5(b). The line now crosses the volume axis below 0. Changes in the gradient of the ESPVR can be

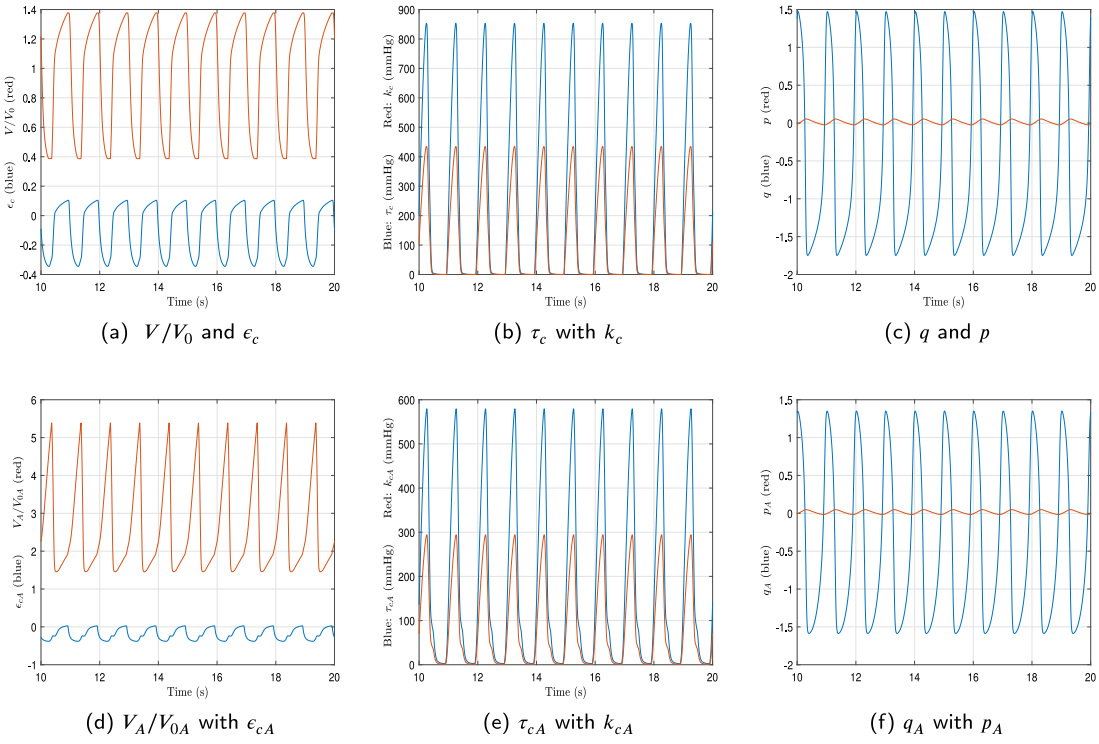

Fig. 4. The ventricular and atrial control case results. Fig. 4(a) shows V/V_0 with ϵ_c. Fig. 4(d) shows V_A/V_{0A} with ϵ_{cA}. Fig. 4(b) shows τ_c with k_c. Fig. 4(e) shows τ_{cA} with k_{cA}. Fig. 4(c) shows q with p. Fig. 4(f) shows q_A with p_A.

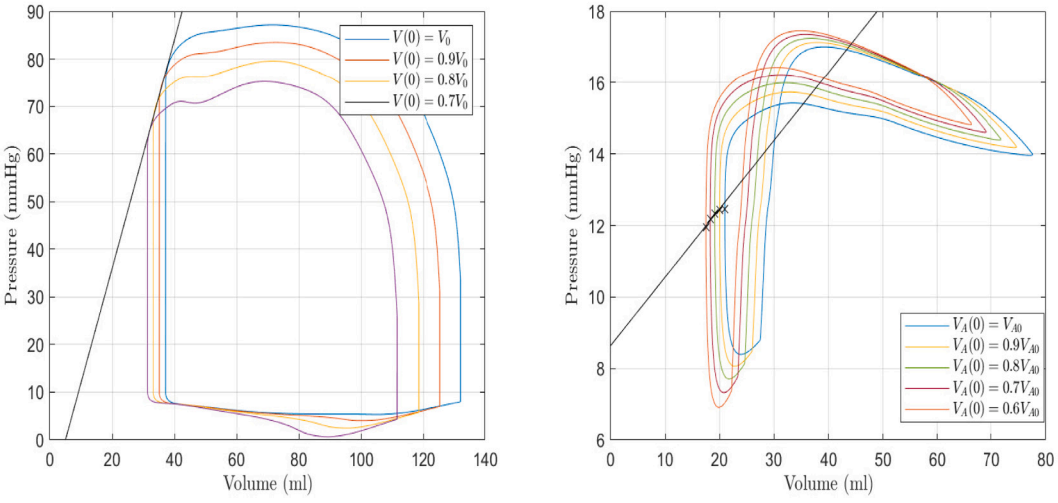

(a) Ventricle P-V loops with different preloads. The line shows the ESPVR.

(b) Atrium P-V loops with different preloads. The line shows the ESPVR.

Fig. 5. The ventricular and atrial P-V loops obtained with different preloads: $V(0) = [1.0, 0.9, 0.8, 0.7]V_0$ for the ventricle and $V_A(0) = [1.0, 0.9, 0.8, 0.7, 0.6]V_{0A}$ for the atrium. The lines in each figure show an approximate ESPVR.

used to asses changes in the inotropic state of the LA [49]. The gradient in the control case here shown in Fig. 5(b) is 0.12 mmHg/ml, which is significantly smaller than that of the ventricle, which is 2.14 mmHg/ml.

3.2. Effects of the left ventricle MEF parameters

In this section, the MEF in the left ventricle is explored by increasing the ventricle parameters μ_1 or μ_2 individually, whilst at the same time keeping the atrial MEF parameters μ_{1A} and μ_{2A} at their respective control values ($\mu_{1A} = 0.0024$, $\mu_{2A} = 0$). Recall that μ_1 mimics systolic stretch and μ_2 the diastolic, and likewise for the atrial μ_{1A} and μ_{2A}. Also, note that they allow the cellular ion channels to be represented, as the opening and closing of these channels would be reflected in the MEF parameter values. Among different cases we have explored, in the following we only show some noteworthy cases.

3.2.1. Effect of the left ventricle MEF parameter μ_1 ($\mu_2 = 0$)

The influence of the MEF parameter μ_1 is now investigated by progressively increasing μ_1 with the other parameters set to their control values in Tables 1 and 2. These results for μ_1 are shown in Fig. 6. The mean ventricle stroke volume (SV - ml), cardiac output (CO - l/min), heart-rate (hr - bps), and power (pw - W) are summarised in Table 5. Control values are available in the top row. Overall, the behaviour of the left ventricle closely follows Kim and Capoccia [32], demonstrating

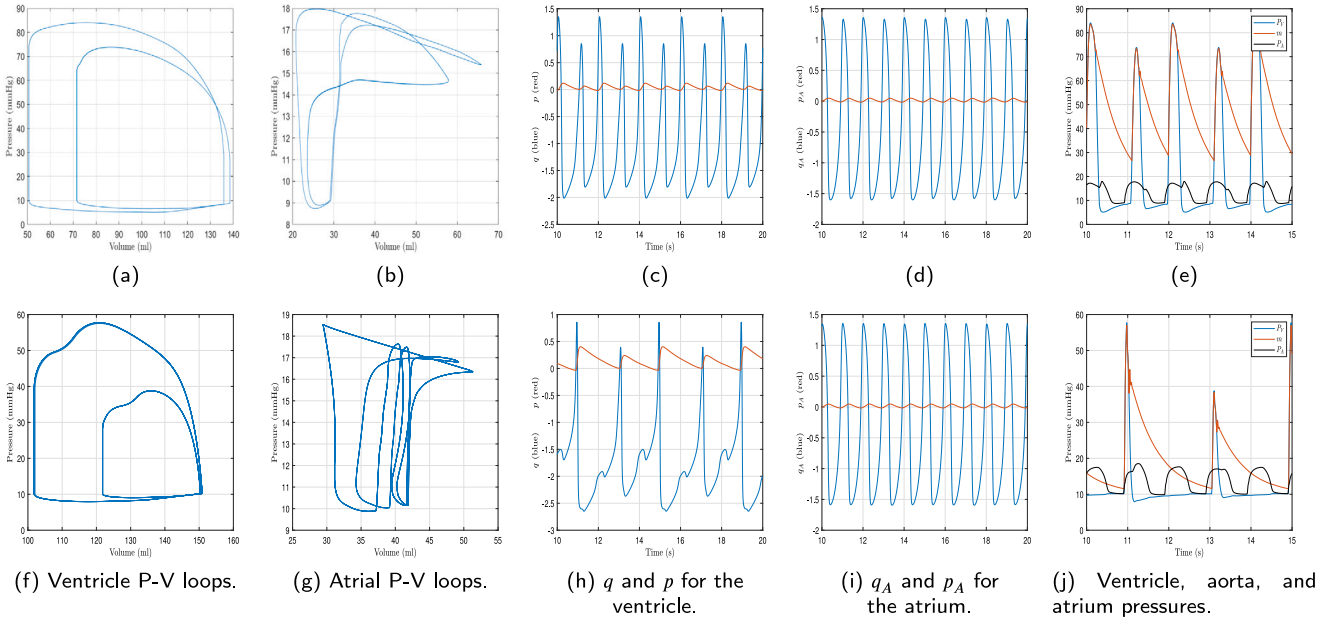

Fig. 6. The effect of increasing μ_1 ($\mu_2 = 0$). Top row: $\mu_1 = 0.0122$, bottom row: $\mu_1 = 0.3$; and from left to right: the ventricle P-V loops, the atrium P-V loop, the ventricle electrical variables, the atrial electric variables, and the ventricle (blue), aorta (red), and atrium (black) pressures.

Table 5
The effect of increasing μ_1 ($\mu_2 = 0$).

μ_1	SV	CO	hr	pw
0.0024	95.00	5.70	1.00	0.93
0.0122	76.12	4.56	1.01	0.65
0.3	38.47	1.14	0.50	0.09

Table 6
The effect of increasing μ_2 ($\mu_1 = 0.0024$).

μ_2	SV	CO	hr	pw
0	95.00	5.70	1.00	0.93
0.3	51.29	6.25	2.04	0.99
1.9	37.45	6.56	2.99	1.06

that the ventricular part of the model is not affected by the presence of the atrium. The values corresponding to period doubling and bifurcation are also found to closely follow Kim and Capoccia. As μ_1 increases, the end-systolic volume rises leading to a decline in power output. The number of oscillations in a given time period also reduces, which contributes to a reduction of power. The fast electrical activity variable reduces in value, whilst the slow activity increases slightly faster and falls progressively slower. This shows that the repolarisation phase of the excitation wave is progressively lengthened, hence the duration of the action potential is prolonged; a result seen by others [20,21]. As the fast activity reduces in magnitude, ventricular and aortic pressure fall too leading to missed ventricle contractions (beats) appearing.

In Figs. 6(e) and 7(j) it can be seen from the atrium pressure trace (black) that the numbers of active atrial contractions appear to be reduced; a reduction of a-phase peaks is clearly seen. On those cycles without active atrial contraction, the passive 'reservoir' phase increases in maximum value as a response. Despite the fall in the number of atrium active contractions, the atrium electrical variables are unaffected by the rise in μ_1. The electrophysiology of the atrium thus appears to be fairly immune to stretch during ventricular systole. The decline in active contractions and change in the $P_A - V_A$ loop are thus a mechanical response to the circulation modification, brought about by the changes in the ventricle.

3.2.2. *Effect of the left ventricle MEF parameter μ_2 ($\mu_1 = 0.0024$)*

μ_1 is put back to the control value ($\mu_1 = 0.0024$) and μ_2 increased to $\mu_2 = 0.3$, and $\mu_2 = 1.9$ (Fig. 7). Again they closely mirror those observed in [32]. As μ_2 is increased, ectopic beats appear. 10 oscillations in 10 s are visible in Fig. 4(c) for the control case, while in the bottom row of Fig. 7, there are 28 oscillations. The heart rate (and other measurements) is provided in Table 6 and more than doubles. Ectopic beats are a common effect of the MEF [32]. Recall that increases in μ_2 increase susceptibility to SAC stimulation during diastolic stretch. Stretch during diastole causes SACs to open, allowing currents to flow into the cell which depolarises the action potential causing contraction [21,36]. These new oscillations cause the P-V loops to become increasingly more complex as evident in Fig. 7(f) in the bottom row. Opposite to the result of a μ_1 increase, the slow electrical variable p reduces and the maximum value of the fast electrical variable q increases due to the additional depolarising currents. The stroke volume of the ventricle falls with rise in μ_2.

As with μ_1, μ_2 appears only to affect the atrial mechanical behaviour. The electrical variables q_A and p_A do not change. In Fig. 7(j), the black line shows the number of atrial contractions does not change, although their character does show slight differences. This can best be seen by observing the small changes in the a-phase peaks of atrial pressure. Overall though, it may be concluded that the main effect of LV MEF on the LA is mechanical (due to its coupling to the LV via circulation), with little influence on the atrial electrophysiology. This is expected from the one-way messaging of the AV node.

3.3. *Effect of atrial MEF parameters*

The MEF parameters for the ventricle are now reset to their respective control values ($\mu_1 = 0.0024$, $\mu_2 = 0$) and those from the atrium are varied to see what effect they have on the ventricle and atrium. Beginning with μ_{1A}, Fig. 8 shows the result of progressively increasing μ_{1A} as $\mu_{1A} = [0.008, 0.8, 80]$. The effect of μ_{1A} on the atrium is similar to the effect of μ_1 on the ventricle. As μ_{1A} increases, the frequency of atrial active contractions falls so the output of the atrium is reduced slightly. Recall the atrium is still mechanically coupled to the ventricle, so the apparent number of atrial 'cycles' does not differ

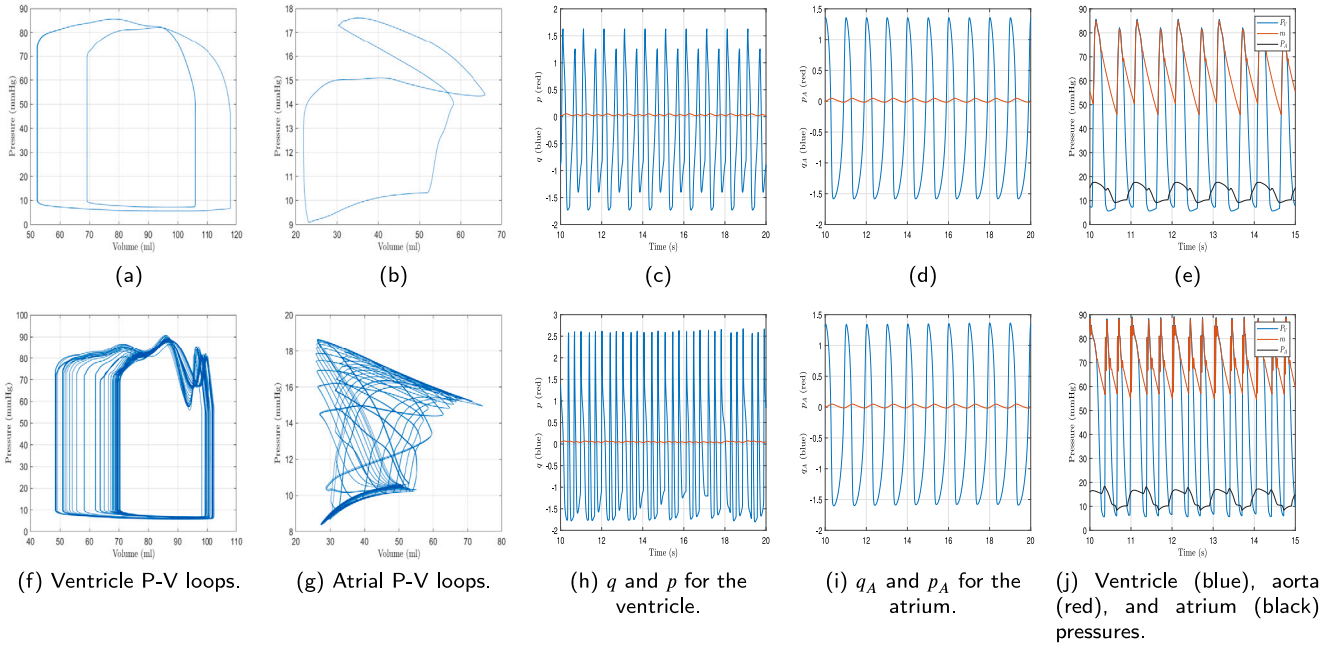

Fig. 7. The effect of increasing μ_2 ($\mu_1 = 0.0024$). Top row: $\mu_2 = 0.3$, bottom row: $\mu_2 = 1.9$; and from left to right: the ventricle P-V loops, the atrium P-V loop, the ventricle electrical variables, the atrial electric variables, and the ventricle (blue), aorta (red), and atrium (black) pressures.

Table 7
The effect of increasing μ_{1A} ($\mu_{2A} = 0$).

μ_{1A}	SV	CO	hr	pw
0.0024	95.00	5.70	1.00	0.93
0.008	95.03	5.70	1.00	0.94
0.8	87.78	5.23	1.00	0.8
80	96.68	4.97	0.85	0.74

Table 8
The effect of increasing μ_{2A} ($\mu_{1A} = 0.0024$).

μ_{2A}	SV	CO	hr	pw
0.0024	95.00	5.70	1.00	0.93
0.2	94.8	5.69	0.99	0.94
20	105.33	5.65	0.89	0.93
200	105.48	5.63	0.88	0.93

from that of ventricle. The fast electrical activity variable q_A reduces in value similar to the ventricle for μ_1, and the slow activity increases faster and falls slower producing a longer action potential (AP) duration consistent with other studies [50,51]. As the electrical signals from the atrium pass to the ventricle, the maximum value of q reduces too, leading to missed (ectopic) beats and a reduction in heart-rate. The heart-rate tends to vary in atrial fibrillation, varying by as much as 200 bpm. Table 7 summarises the mean ventricle heart-rate, cardiac output, stroke volume, and power. The mean cardiac output can be seen to fall from 5.70 l/min in the control case to 4.97 l/min when $\mu_{1A} = 80$. Cardiac output reductions are a common symptom of irregular ventricular rhythm during atrial arrhythmia [52]. Likewise the mean power falls from 0.93 W in the control case to 0.74 W.

In order to establish the influence of atrial MEF parameter μ_{2A}, μ_{1A} is returned to its control value ($\mu_{1A} = 0.0024$) and μ_{2A} increased as $\mu_{2A} = [0.2, 20, 200]$. As μ_{2A} rises, the active a-phase of the atrial cycle dominates the passive v-phase and the maximum value of the pressure increases. From Figs. 9(e), 9(j), and 9(o) the peak in the black trace denoting atrial pressure increases, showing that the active atrial contractions grows in strength. Table 8 shows the ventricular stroke volume, cardiac output and heart-rate. Interestingly, the number of ventricular oscillations reduces as evident from the table and the ventricular electric variables fluctuations. This may be due to the rise of p_A in value, so the atrium AP no longer repolarises, reducing the frequency of AV node signals to the ventricle. The stroke volume of the ventricle is not significantly modified, but the maximum pressure of both the ventricle and atrium increases.

Left AFib and arrhythmia are associated with higher pressures [28, 53] and atrial dilation [15], although it would be difficult to equate the results here with AFib due to a slightly lower atrial rhythm. The heart-rate reduces from 60 bpm to 52.8 bpm (for $\mu_{2A} = 200$), and the cardiac output reduces slightly to 5.63 l/min as evident in the Table 8. The reduction in the mean heart-rate stands in contrast to μ_2 which increased the heart-rate in the ventricle. The power is not altered, as the systolic ventricular pressure increases, compensating for the reduced heart-rate. Overall, it appears μ_{2A} does not affect the heart to the same degree as μ_{1A}. A higher atrial rhythm and AFib cannot be induced using μ_{2A}, whilst μ_{1A} reduces the heart-rate in both ventricle and atrium. In summary, diastolic stretch of the atrium prevents repolarisation of the action potential, which consequently remains in a perpetually depolarised state; reducing then eliminating the passive v-phase of the atrium. The heart-rate falls slightly due to the reduction in electrical signals coming from the atrium.

4. Discussion

The aim of this study was to develop a model of the heart which consistently evolves the LA and LV. The model for the left ventricle developed by Kim and Capoccia [31,32] is extended to include an additional elastic chamber (the LA) upstream. By using a similar myocyte model for the atrium as that used for the ventricle, the approach here develops the macro-scale atrial contractile mechanics from the behaviour of the atrial micro-scale myofibers, without reference to the time-varying-elastance method, thereby allowing the study of the MEF. The TVE approach prescribes the ventricle and atrial pressure–volume relationship directly using a periodic function based on physiological values. It neglects the micro-scale cellular and electrical dynamics responsible for the chamber behaviour. Physiological feedback and regulating mechanisms are overlooked so it cannot be used to simulate the MEF. Importantly for this study it has yet to be validated for

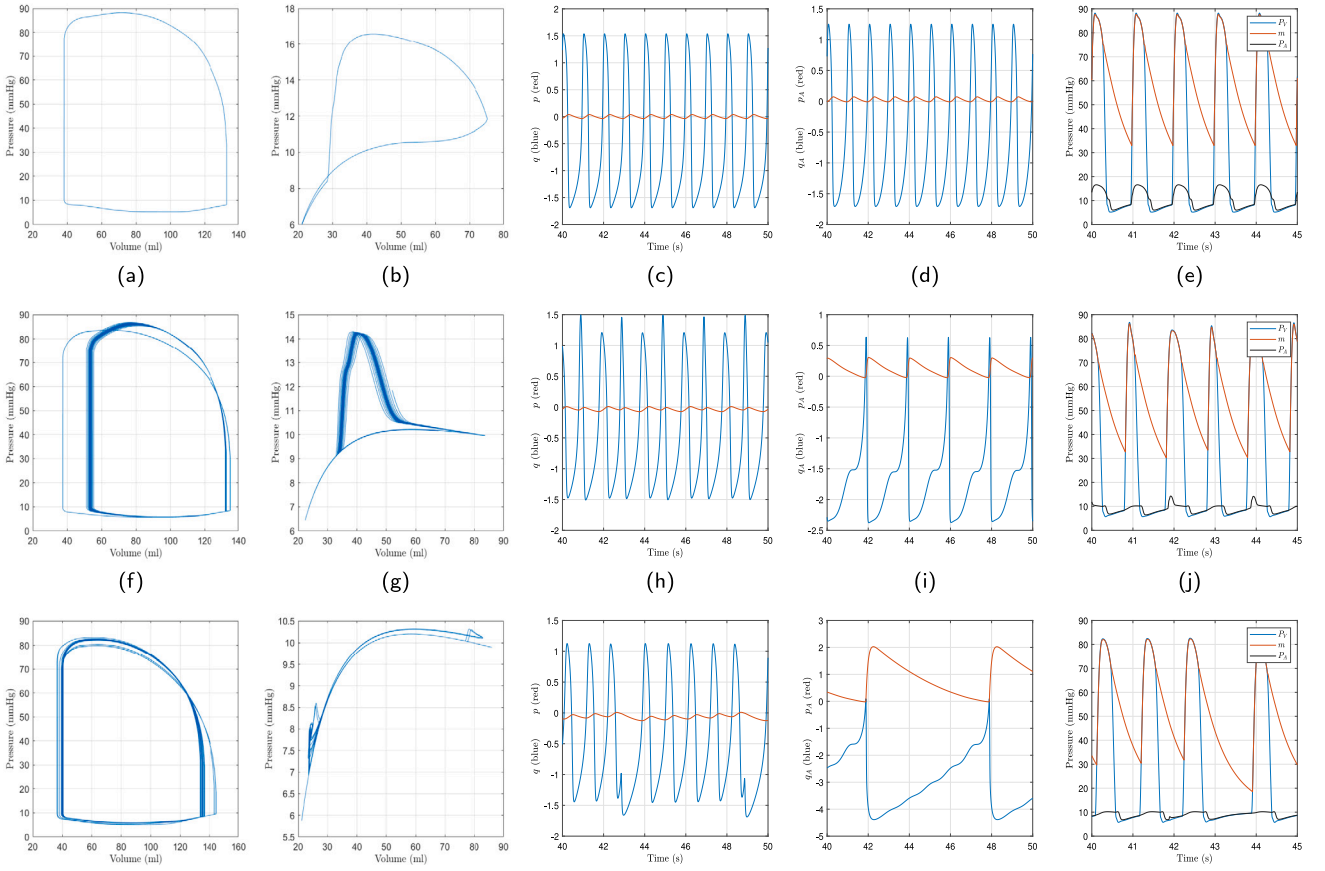

Fig. 8. The effect of increasing μ_{1A} ($\mu_{2A} = 0$). Top row: $\mu_{1A} = 0.008$, second row: $\mu_{1A} = 0.8$, bottom row: $\mu_{1A} = 80$. From left to right: the ventricle P-V loops (8(a), 8(f), 8(k)), the atrium P-V loop (8(b), 8(g), 8(l)), the ventricle electrical variables (8(c), 8(h), 8(m)), the atrial electric variables (8(d), 8(i), 8(n)), and the ventricle (blue), aorta (red), and atrium (black) pressures (8(e), 8(j), 8(o)). The change in time-scales to figures above is due to initial transients persisting for longer.

the atrium. By considering multiple scales and domains our model acquires a synergistic quality allowing the MEF and the cellular activity to be explored. The atrial model myocyte parameters differ from the ventricle to reflect physical differences between the two [39]. The function of the AV node is captured in the model by passing the atrial electrical messaging from the SAN node into the ventricle electrical model, simulating the AP conduction pathway.

In the controlled case representing a healthy resting heart, the resulting atrial behaviour shows the characteristic 2-phase response with both the active contraction and passive 'reservoir' phases represented. The active a-phase appears soon in the cardiac cycle such that the a-loop in the atrial pressure–volume plot appears distended downwards and the reservoir phase reaches large values of volume. The conduit period of the atrium cycle is not represented though, as this period is a result of pressure wave propagation; effects that cannot be captured by the model [49]. Extension of the model in a spatial direction would allow a basic representation of the conduit phase. This may change the results, or cause new effects resulting from the MEF, as spatio-temporal dynamics affect MEF behaviour. Whilst the atrial pressure magnitude is representative of a human left-atrium, the volume tends to be large although it is similar in range to the results from other computational models of the human heart [4,39]. Nevertheless, our model reproduced the key features of the atrium dynamics such as the end-systolic pressure–volume relation while permitting us to examine the MEF. Not shown in the results is how the variation of the delay between atrial and ventricle contractions, reflected by the parameter s, changes the pressure–volume appearance of the atrium.

By including additional parameters that capture the effects of systolic and diastolic cell stretch, an investigation of the MEF in the ventricle and atrium is carried out. The effects of atrial and ventricular systolic stretch on the action potential is modelled by introducing an additional parameter that couples the cell stresses into the electrical models of each chamber. Likewise, the effects of diastolic stretch are modelled by coupling the electrical models to increases in the chamber volume. Systolic stretch of the ventricle is observed to increase the action potential duration by prolonging the repolarisation phase of the action potential. This is a known side effect of systolic stretch [19–21], and has been observed by Kim and Capoccia [32] in the original ventricle model. Further, missed ventricle beats occur, as evidenced by the reduction of heart-rate, and periodic behaviour is seen as shown by the repeated loops in the pressure–volume diagram. Diastolic stretch of the ventricle causes the AP to depolarise, consistent with [15,20–22] who saw similar effects. Ectopic beats appear too as SACs are opened causing the AP to depolarise and the initiation of a new ventricle contraction.

For the atrium, systolic stretch of the ventricles reduces the numbers of active atrial contractions and the pressure–volume loop of the atrium is modified. It does not change the electrophysiology of the atrium though, so the changes are thought to be caused by the modified circulation. A reduction of the blood supply to the atrium for example, would lower the atrial stretch, leading to a fall in active contractions. Diastolic stretch of the ventricle leads to variations in the a and v phases of the atrium, but no consistent pattern develops as the MEF disorder worsens (μ_2 rises). Like systolic stretch, diastolic stretch of the

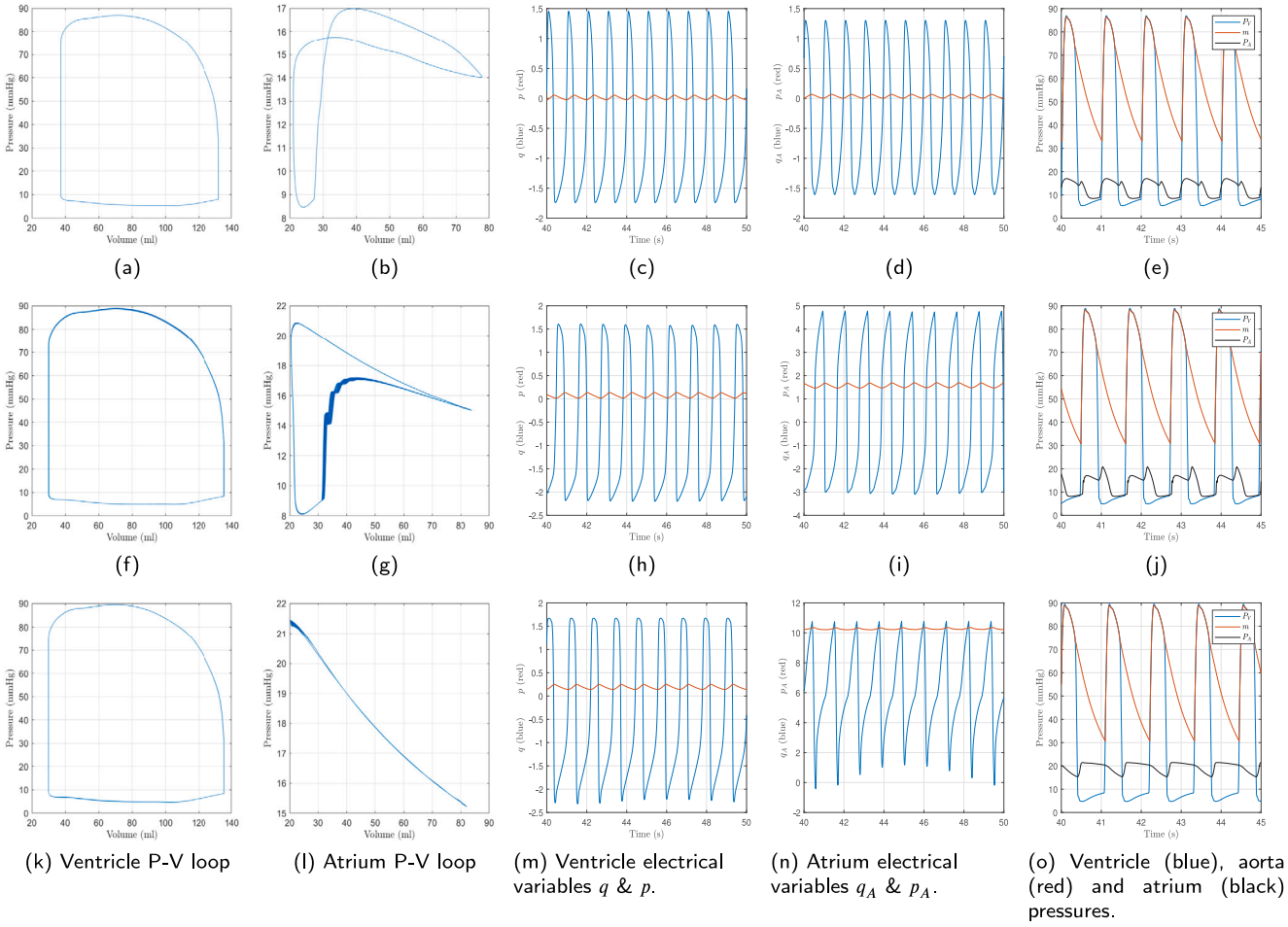

Fig. 9. The effect of increasing μ_{2A} ($\mu_{1A} = 0.0024$). Top row: $\mu_{2A} = 0.2$, second row: $\mu_{2A} = 20$, bottom row: $\mu_{2A} = 200$. From left to right: the ventricle P-V loops (9(a), 9(f), 9(k)), the atrium P-V loop (9(b), 9(g), 9(l)), the ventricle electrical variables (9(c), 9(i), 9(n)), the atrial electric variables (9(c), 9(i), 9(n)), and the ventricle (blue), aorta (red), and atrium (black) pressures (9(e), 9(j), 9(o)).

ventricle does not change the electrophysiology of the atrium. This is unsurprising given the one-way conduction path for the AP.

Systolic stretch of the atrium in the presence of MEF disorder reduces the frequency of atrial active contractions and output. The depolarisation of the AP reduces in magnitude and the repolarisation phase takes longer, increasing the AP duration similar to the ventricle. Changes in the atrial AP duration with stretch have been observed experimentally [50,51]. For instance [51] observed that stretch increased the late duration of the AP when the AP was at 90% repolarisation. The depolarisation of the ventricle also reduces in frequency leading to missed ectopic beats and a fall in heart-rate, cardiac output and the pumping power of the heart. Atrial arrhythmia is therefore confirmed to degrade heart function and may lead to negative consequences for patient health. Diastolic stretch of the atrium, however, does not harm the ventricle to the same extent as systolic stretch, producing only a slight reduction in heart-rate. The magnitude of the atrial electric variables increases, consistent with experimental results showing an increase in AP magnitude induced by atrial stretch [50]. Fibrillation of the left atrium was not seen with diastolic atrial stretch, in contrast to diastolic stretch of the ventricle. This result stands in contrast to studies showing AFib susceptibility increases with atrial stretch.

Finally, we note that the lumped-parameter design of the model presented is limited by the omission of spatio-temporal mechanics, hence effects such as pressure wave propagation cannot be modelled, so the conduit 'c' wave in the atrium pressure is absent. The lack of spatial mechanics also has consequences for the MEF which limits its usefulness in the study of arrhythmia, as wave propagation has effects in the electrophysiological behaviour [54]. An expansion of the model to spatial dimensions will be left for further study. The model includes two electrical models; one for the ventricle and one for the atrium. A further limitation of the current model is the number of parameters which require definition. Incorrect values of the parameters leads to inaccurate or unrealistic behaviour. We intend to use our model initially to study disease and artefacts of the AV node such as a heart block. We will also extend our model to spatial dimensions such that the conduit period of the atrium behaviour is reproduced and spatio-temporal effects of the MEF can be simulated.

5. Conclusion

The model presented is simple enough to be intuitive and accessible within the clinical environment, yet it contains enough detail to study complex cardiac behaviour such as the mechano-electric feedback (MEF), overcoming the limitations of popular time-varying elastance (TVE) approach. Specifically, the inclusion of the atrium in the synergistic cardiovascular systems makes it one of the few atrial numerical models that does not make reference to the TVE method. The model is able to produce the essential features of atrial behaviour such as the figure-of-eight pressure volume loop. The MEF mechanism is studied and its effects noted in both the left ventricle and atrium. MEF in the ventricle prolongs the repolarisation phase of the action potential and can cause missed or ectopic beats depending on when stretch is applied. MEF in the atrium detriments heart function by reducing cardiac power, output and heart-rate. Further study of the atrium MEF

could therefore be beneficial to patients suffering complications in the atrium. Our model will also be useful for the modelling of heart defects such as valve problems [4] and diseases of the AV node such as node block.

CRediT authorship contribution statement

Nicholas F. Pearce: Conceptualization, Methodology, Formal analysis, Writing. **Mark C. Turner:** Reviewing and editing. **Eun-jin Kim:** Conceptualization, Methodology, Writing, Supervision.

Declaration of competing interest

The authors declare that they have no known competing financial interests or personal relationships that could have appeared to influence the work reported in this paper.

References

[1] WHO, Centers for disease control and prevention, national center for health statistics, about multiple cause of death, 1999–2019, 2022, https://www.who.int/news-room/fact-sheets/detail/the-top-10-causes-of-death. (Accessed 10 April 2022).

[2] Centers for disease control and prevention, national center for health statistics, about multiple cause of death, 1999–2019, 2022, https://wonder.cdc.gov/mcd-icd10.html. (Accessed 28 May 2022).

[3] T.B.H. Foundation, 2022, https://www.bhf.org.uk/informationsupport/conditions/atrial-fibrillation. (Accessed 14 May 2022).

[4] T. Korakianitis, Y. Shi, A concentrated parameter model for the human cardiovascular system including heart valve dynamics and atrioventricular interaction, Med. Eng. Phys. 28 (7) (2006) 613–628.

[5] E.-O. Jung, W.-H. Lee, Lumped parameter models of cardiovascular circulation in normal and arrhythmia cases, J. Korean Math. Soc. 43 (4) (2006) 885–897.

[6] S. Bozkurt, Mathematical modeling of cardiac function to evaluate clinical cases in adults and children, PLoS One 14 (10) (2019) e0224663.

[7] T. Heldt, Computational Models of Cardiovascular Response to Orthostatic Stress (Ph.D. thesis), Massachusetts Institute of Technology, 2004.

[8] T.E. Claessens, D. Georgakopoulos, M. Afanasyeva, S.J. Vermeersch, H.D. Millar, N. Stergiopulos, N. Westerhof, P.R. Verdonck, P. Segers, Nonlinear isochrones in murine left ventricular pressure-volume loops: how well does the time-varying elastance concept hold? Am. J. Physiol. Heart Circul. Physiol. 290 (4) H1474–H1483.

[9] A. Pironet, P.C. Dauby, S. Paeme, S. Kosta, J.G. Chase, T. Desaive, Simulation of left atrial function using a multi-scale model of the cardiovascular system, PLoS One 8 (6) (2013) e65146.

[10] K.T.V. Koon, V. Le Rolle, G. Carrault, A. Hernández, A cardiovascular model for the analysis of pacing configurations in cardiac resynchronization therapy, in: 2009 36th Annual Computers in Cardiology Conference, CinC, IEEE, 2009, pp. 393–396.

[11] S. Noreen, A. Ben-Tal, M. Elstad, W.L. Sweatman, R. Ramchandra, J. Paton, Mathematical modelling of atrial and ventricular pressure–volume dynamics and their change with heart rate, Math. Biosci. 344 (2022) 108766.

[12] J. Alexander Jr., K. Sunagawa, N. Chang, K. Sagawa, Instantaneous pressure-volume relation of the ejecting canine left atrium, Circ. Res. 61 (2) (1987) 209–219.

[13] B.D. Hoit, Y. Shao, M. Gabel, R.A. Walsh, In vivo assessment of left atrial contractile performance in normal and pathological conditions using a time-varying elastance model, Circulation 89 (4) (1994) 1829–1838.

[14] B. Su, X. Wang, F. Kabinejadian, C. Chin, T.T. Le, J.-M. Zhang, Effects of left atrium on intraventricular flow in numerical simulations, Comput. Biol. Med. 106 (2019) 46–53.

[15] T.A. Quinn, P. Kohl, Cardiac mechano-electric coupling: acute effects of mechanical stimulation on heart rate and rhythm, Physiol. Rev. 101 (1) (2021) 37–92.

[16] A. Quarteroni, T. Lassila, S. Rossi, R. Ruiz-Baier, Integrated heart—coupling multiscale and multiphysics models for the simulation of the cardiac function, Comput. Methods Appl. Mech. Engrg. 314 (2017) 345–407.

[17] P. Kohl, P. Hunter, D. Noble, Stretch-induced changes in heart rate and rhythm: clinical observations, experiments and mathematical models, Prog. Biophys. Mol. Biol. 71 (1) (1999) 91–138.

[18] Z. Knudsen, A. Holden, J. Brindley, Qualitative modeling of mechanoelectrical feedback in a ventricular cell, Bull. Math. Biol. 59 (6) (1997) 1155–1181.

[19] S.N. Healy, A.D. McCulloch, An ionic model of stretch-activated and stretch-modulated currents in rabbit ventricular myocytes, Ep Europace 7 (s2) (2005) S128–S134.

[20] T.A. Quinn, H. Jin, P. Lee, P. Kohl, Mechanically induced ectopy via stretch-activated cation-nonselective channels is caused by local tissue deformation and results in ventricular fibrillation if triggered on the repolarization wave edge (commotio cordis), Circulation: Arrhythm. Electrophysiol. 10 (8) (2017) e004777.

[21] T.L. Riemer, E.A. Sobie, L. Tung, Stretch-induced changes in arrhythmogenesis and excitability in experimentally based heart cell models, Am. J. Physiol.-Heart Circ. Physiol. 275 (2) (1998) H431–H442.

[22] P. Kohl, C. Bollensdorff, A. Garny, Effects of mechanosensitive ion channels on ventricular electrophysiology: experimental and theoretical models, Exp. Physiol. 91 (2) (2006) 307–321.

[23] F. Solti, T. Vecsey, V. Kekesi, A. Juhasz-Nagy, The effect of atrial dilatation on the genesis of atrial arrhythmias, Cardiovasc. Res. 23 (10) (1989) 882–886.

[24] F.J. Chorro, S. Egea, L. Mainar, J. Cánoves, J. Sanchis, E. Llavador, V. López-Merino, L. Such, Modificaciones agudas de la longitud de onda del proceso de activación auricular inducidas por la dilatación. Estudio experimental, Rev. Esp. Cardiol. 51 (11) (1998) 874–883.

[25] S.C. Eijsbouts, M. Majidi, M.v. Zandvoort, M.A. Allessie, Effects of acute atrial dilation on heterogeneity in conduction in the isolated rabbit heart, J. Cardiovasc. Electrophysiol. 14 (3) (2003) 269–278.

[26] S.C. Eijsbouts, R.P. Houben, Y. Blaauw, U. Schotten, M.A. Allessie, Synergistic action of atrial dilation and sodium channel blockade on conduction in rabbit atria, J. Cardiovasc. Electrophysiol. 15 (12) (2004) 1453–1461.

[27] J. Li, J. Xiao, D. Liang, H. Zhang, G. Zhang, Y. Liu, Y. Zhang, Y. Liu, Z. Yu, B. Yan, et al., Inhibition of mitochondrial translocator protein prevents atrial fibrillation, Eur. J. Pharmacol. 632 (1–3) (2010) 60–64.

[28] A. Antoniou, D. Milonas, J. Kanakakis, S. Rokas, D.A. Sideris, Contraction-excitation feedback in human atrial fibrillation, Clin. Cardiol. 20 (5) (1997) 473–476.

[29] F. Ravelli, M. Masè, M. Del Greco, M. Marini, M. Disertori, Acute atrial dilatation slows conduction and increases AF vulnerability in the human atrium, J. Cardiovasc. Electrophysiol. 22 (4) (2011) 394–401.

[30] P. Brocklehurst, H. Ni, H. Zhang, J. Ye, Electro-mechanical dynamics of spiral waves in a discrete 2D model of human atrial tissue, PLoS One 12 (5) (2017) e0176607.

[31] E.-j. Kim, M. Capoccia, Synergistic model of cardiac function with a heart assist device, Bioengineering 7 (1) (2019) 1.

[32] E.-j. Kim, M. Capoccia, Mechano-electric effect and a heart assist device in the synergistic model of cardiac function, Math. Biosci. Eng. 17 (5) (2020) 5212–5233.

[33] M.B. Jamshidi, J. Talla, Z. Peroutka, Deep learning techniques for model reference adaptive control and identification of complex systems, in: 2020 19th International Conference on Mechatronics - Mechatronika, ME, 2020, pp. 1–7, http://dx.doi.org/10.1109/ME49197.2020.9286698.

[34] H. Keshmiri Neghab, M.B. Jamshidi, H. Keshmiri Neghab, Digital twin of a magnetic medical microrobot with stochastic model predictive controller boosted by machine learning in cyber-physical healthcare systems, Information 13 (7) (2022) URL: https://www.mdpi.com/2078-2489/13/7/321.

[35] N. Pearce, E.-j. Kim, Modelling the cardiac response to a mechanical stimulation using a low-order model of the heart, Math. Biosci. Eng. 18 (4) (2021) 4871–4893.

[36] G. Tse, S.T. Wong, V. Tse, Y.T. Lee, H.Y. Lin, J.M. Yeo, Cardiac dynamics: alternans and arrhythmogenesis, J. Arrhythmia 32 (5) (2016) 411–417.

[37] P. Colli Franzone, L.F. Pavarino, S. Scacchi, Effects of mechanical feedback on the stability of cardiac scroll waves: A bidomain electro-mechanical simulation study, Chaos 27 (9) (2017) 093905, http://dx.doi.org/10.1063/1.4999465, http://dx.doi.org/10.1063/1.4999465.

[38] A. Collet, J. Bragard, P. Dauby, Temperature, geometry, and bifurcations in the numerical modeling of the cardiac mechano-electric feedback, Chaos 27 (9) (2017) 093924.

[39] J. Walklate, C. Ferrantini, C.A. Johnson, C. Tesi, C. Poggesi, M.A. Geeves, Alpha and beta myosin isoforms and human atrial and ventricular contraction, Cell. Mol. Life Sci. 78 (23) (2021) 7309–7337.

[40] J. Bestel, Modèle différentiel de la contraction musculaire contrôlée: Application au système cardio-vasculaire (Ph.D. thesis), Paris 9, 2000.

[41] J. Bestel, F. Clément, M. Sorine, A biomechanical model of muscle contraction, in: International Conference on Medical Image Computing and Computer-Assisted Intervention, Springer, 2001, pp. 1159–1161.

[42] P. Krejci, J. Sainte-Marie, M. Sorine, J. Urquiza, Modelling and simulation of an active fibre for cardiac muscle, Biomech. Model. Mechanobiol. (2006).

[43] A.M. Katz, Physiology of the Heart, Lippincott Williams & Wilkins, 2010.

[44] D.A. Rowen, A.D. Likens, N. Stergiou, Revisiting a classic: Muscles, reflexes, and locomotion by McMahon, J. Biomech. Gait Anal. (2020) 149–224.

[45] A. Huxley, Muscular contraction, J. Physiol. 243 (1) (1974) 1.

[46] A. Amar, S. Zlochiver, O. Barnea, Mechano-electric feedback effects in a three-dimensional (3D) model of the contracting cardiac ventricle, PLoS One 13 (1) (2018) e0191238.

[47] R. FitzHugh, Impulses and physiological states in theoretical models of nerve membrane, Biophys. J. 1 (6) (1961) 445–466.

[48] A. Roka, Atrioventricular conduction in atrial fibrillation: Pathophysiology and clinical implications, Atrial Fibrillation-Basic Res. Clin. Appl. (2012).

[49] P.S. Pagel, F. Kehl, M. Gare, D.A. Hettrick, J.R. Kersten, D.C. Warltier, Mechanical function of the left atrium: new insights based on analysis of pressure–volume relations and Doppler echocardiography, J. Am. Soc. Anesthesiol. 98 (4) (2003) 975–994.

[50] P. Tavi, M. Laine, M. Weckstrom, Effect of gadolinium on stretch-induced changes in contraction and intracellularly recorded action-and afterpotentials of rat isolated atrium, Br. J. Pharmacol. 118 (2) (1996) 407–413.

[51] P. Tavi, C. Han, M. Weckstrom, Mechanisms of stretch-induced changes in [Ca2+] i in rat atrial myocytes: role of increased troponin C affinity and stretch-activated ion channels, Circ. Res. 83 (11) (1998) 1165–1177.

[52] D.M. Clark, V.J. Plumb, A.E. Epstein, G. Kay, Hemodynamic effects of an irregular sequence of ventricular cycle lengths during atrial fibrillation, J. Am. Coll. Cardiol. 30 (4) (1997) 1039–1045, http://dx.doi.org/10.1016/S0735-1097(97)00254-4, URL: https://www.sciencedirect.com/science/article/pii/S0735109797002544.

[53] C.W. White, R.E. Kerber, H.R. Weiss, M.L. Marcus, The effects of atrial fibrillation on atrial pressure-volume and flow relationships, Circ. Res. 51 (2) (1982) 205–215.

[54] Z. Qu, G. Hu, A. Garfinkel, J.N. Weiss, Nonlinear and stochastic dynamics in the heart, Phys. Rep. 543 (2) (2014) 61–162.